Medical Physics
The International Journal of Medical Physics Research and Practice

Exploring potential mechanisms responsible for observed changes of ultrasonic backscattered energy with temperature variations

Xin Li, Goutam Ghoshal, Roberto J. Lavarello, and Michael L. Oelze

Citation: Medical Physics **41**, 052901 (2014); doi: 10.1118/1.4870964
View online: http://dx.doi.org/10.1118/1.4870964
View Table of Contents: http://scitation.aip.org/content/aapm/journal/medphys/41/5?ver=pdfcov
Published by the American Association of Physicists in Medicine

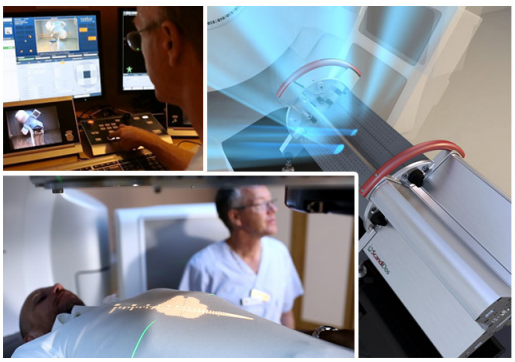

Exploring potential mechanisms responsible for observed changes of ultrasonic backscattered energy with temperature variations

Xin Li
Department of Nuclear, Plasma, and Radiological Engineering, University of Illinois at Urbana-Champaign, Urbana, Illinois 61801

Goutam Ghoshal
Department of Electrical and Computer Engineering, University of Illinois at Urbana-Champaign, Urbana, Illinois 61801

Roberto J. Lavarello
Seccion Electricidad y Electronica, Pontificia Universidad Catolica del Peru, San Miguel, Lima 32, Peru

Michael L. Oelze[a)]
Department of Electrical and Computer Engineering, University of Illinois at Urbana-Champaign, Urbana, Illinois 61801

(Received 19 September 2013; revised 9 February 2014; accepted for publication 26 March 2014; published 15 April 2014)

Purpose: Previous studies have provided the observation that the ultrasonic backscattered energy from a tissue region will change due to a change of temperature. The mechanism responsible for the changes in backscattered energy (CBE) with temperature has been hypothesized to be from the changes in scattering properties of local aqueous and lipid scatterers. An alternative mechanism is hypothesized here to be capable of producing similar CBE curves, i.e., changes in speckle resulting from changes in summation of scattered wavelets.
Methods: Both simulations and experiments were conducted with a 5.5 MHz, 128-element linear array and synthetic and physical phantoms containing randomly spaced scatterers. The speckle pattern resulting from summation of scattered wavelets was changed in simulations and experiments by directly increasing the background sound speed from 1520 to 1540 m/s, and changing the temperature from 37 °C to 48 °C, respectively. Shifts in the backscattered signal were compensated using 2D cross-correlation techniques.
Results: Excellent agreement between simulations and experiments was observed, with each pixel in the CBE images on average undergoing either a monotonic increase (up to 3.2 dB) or a monotonic decrease (down to −1.9 dB) with increasing sound speed or temperature. Similar CBE curves were also produced by shifting the image plane in the elevational and axial directions even after correcting for apparent motion.
Conclusions: CBE curves were produced by changing the sound speed or temperature in tissue mimicking phantoms or by shifting the image plane in the elevational and axial directions and the production of these CBE curves did not require the presence of lipid and aqueous scatterers.
 [http://dx.doi.org/10.1118/1.4870964]

Key words: change in backscatter energy, ultrasonic thermometry

1. INTRODUCTION

Hyperthermia in the range of 40 °C – 44 °C has been employed in cancer treatment for its ability to synergistically enhance the effects of chemotherapy and radiotherapy, thus reducing the chemical or radiation dosage.[1–5] Noninvasive monitoring and mapping of temperature is important for hyperthermia and ablative therapy techniques.[6,7] Various imaging modalities have been examined for their ability to monitor temperature. For example, x-ray computed tomography (CT), magnetic resonance imaging (MRI), and ultrasound have been explored for their ability to estimate and map temperature.[6–10] Both CT and MRI can provide the sensitivity and spatial resolution needed to map temperature (i.e., fraction of °C at <1 cm spatial resolution). However, the radiation exposure from repeated CT measurements reduces its applicability for real-time monitoring of temperature for hyperthermia or ablative treatment[8] and MRI suffers from high cost and incompatibility with certain devices used for thermal therapy.

Among acoustic thermometry, there exist several methods for estimating temperature from backscattered signals. Most of these methods, however, require prior knowledge of the thermal expansion coefficient and the speed of sound (SOS) dependence on temperature for a specific tissue.[11–13] The most common technique is to estimate the temperature-dependent echo shifts due to changes in SOS and tissue expansion.[11–18] Another method based on ultrasonic signals is to correlate temperature elevation with changes in the backscattered energy (CBE).[19–23] The CBE has been hypothesized to be produced by changes in the local scattering from lipid and aqueous scatterers in the tissues versus

temperature.[19–21] According to the hypothesis, the temperature changes would produce a decrease in the CBE for regions dominated by aqueous scatterers and an increase in the CBE for regions dominated by lipid scatterers.[19]

While this mechanism may help elucidate the CBE observed in tissues due to temperature elevations, other mechanisms may also contribute significantly to the CBE. In this study, it is hypothesized that the CBE could also be attributable to local changes in summation of ultrasonic pulses scattered from subresolution scatterers and not necessarily changes in their scattering cross section. Changes in the summation of the scattered wavelets can be due to at least two factors: changes in SOS with temperature, and movement of the scanning plane between acquisitions of image frames. As the sound speed changes, the time of arrival of scattered wavelets from scatterers will change resulting in a change in the speckle pattern as the wavelets are summed back at the transducer. Furthermore, as the sound speed changes, so does the wavelength of ultrasound. The change in the wavelength can result in a change in the destructive and constructive interference resulting in a change in the speckle pattern. To test this hypothesis, both simulations and experiments were conducted with phantoms that contained scatterers of the same type, e.g., glass bead phantoms, avoiding the coexistence of lipid and aqueous scatterers. By choosing phantoms with only one type of scatterer, the CBE resulting from changes in sound speed or shifting of the scanning plane could be examined separately from CBE effects resulting from having both lipid and aqueous scatterers present.

2. THEORY

Speckle in ultrasound arises from the interference caused by ultrasonic pulses scattered from many subresolution scatterers summed at the transducer.[24,25] The speckle pattern depends on different factors, such as the resolution cell size, the pulse length, shape, and center frequency, and the concentration and spatial organization of the scatterers. By changing the interference pattern, destructive interference (i.e., a local decrease in the signal amplitude) or constructive interference (i.e., an increase in the local signal amplitude) can occur.

Many mechanisms can lead to a change in speckle pattern. For example, changes in the propagation speed of the background medium will modify both the arrival times of individual backscattered echoes and the diffraction of the beam associated with the transducer. These changes will in turn lead to a modified backscattered signal received by the transducer. Alternatively, tissue or transducer motion will cause a change in the location of each scatterer relative to the transducer and therefore will modify the overall backscattered data. Although motion in the lateral direction could be accounted for by proper registration, motion in the axial and in the elevational directions may result in a change in speckle pattern that cannot be entirely accounted for by registration. Both mechanisms, therefore, have the potential to influence the CBE.

3. METHODS

3.A. CBE calculation

Conventionally, the CBE is calculated by comparing the intensity of an image acquired from a sample at a particular temperature with a reference image from the same sample at 37 °C.[22,23] In studies where the SOS changed, before performing the frame-to-frame comparison, it was necessary to register the images to account for apparent motion in the imaging plane. The registration was required because of the change in SOS, which effectively moved the location of the scatterers to be closer to the transducer as the SOS increased. In the current study, two separate 2D cross-correlation methods were explored to align the images prior to CBE calculation.[26,27] In the first method, rigid registration using cross-correlation was used to track a 13.3 × 28.2 mm box within the phantom. The tracking method was used to search in the vicinity of the previous frame by ±200 μm in the axial direction and ±300 μm in the lateral direction. CBE values were calculated for every pixel inside the box. In the second method, nonrigid registration was used. A small 3 × 3 pixel window was used to track the displacement of each individual pixel. For an image frame, each 3 × 3 pixel window was compared to the previous frame using a search of ±10 pixels in axial direction and ±2 pixels in lateral dimension to register the image. For both registration methods, the size of the search region was chosen to be short but larger than the expected frame-to-frame displacements in order to ensure convergence of the cross-correlation operation.

After registration and envelope detection, the pixel values were squared to determine the backscattered energy at each pixel in the image. The CBE in dB was calculated as

$$\mathrm{CBE}_T(i,j) = 10\log_{10}\frac{\mathrm{env}_T{}^2(i,j)}{\mathrm{env}_{37^\circ\mathrm{C}}{}^2(i,j)}, \tag{1}$$

where $\mathrm{env}_T(i,j)$ stands for the value of the envelope at pixel coordinate (i,j) and temperature T. The envelope of the signal was detected by taking the absolute value of the analytic signal acquired from the Hilbert transform of the received signal. Pixels with positive and negative CBE values correspond to an increase and decrease in the pixel energy with respect to the reference at 37°, respectively. A map of the CBE was constructed for each frame at each pixel location with the pixel color corresponding to the CBE value in dB at the spatial location. The positive and negative CBE curves were calculated by averaging the values of all the positive and negative CBE pixels, respectively, i.e.,

$$\mathrm{CBE}_{\mathrm{positive}}(T) = \mathrm{mean}(\{\mathrm{CBE}_T(i,j) > 0\})$$

$$\mathrm{CBE}_{\mathrm{negative}}(T) = \mathrm{mean}(\{\mathrm{CBE}_T(i,j) < 0\}). \tag{2}$$

3.B. Simulation setup

Backscattered data were simulated using FIELD II.[28,29] The simulated array had 128 elements, a length of 3.8 cm, and a center frequency of 5.5 MHz. The element height and elevation focus were set to 4 and 16 mm, respectively. The

numerical phantoms consisted of identical point scatterers randomly distributed spatially in a region of 40 mm width, 15 mm length, and 3.5 mm thickness at a concentration of ten scatterers per resolution cell in order to produce fully developed speckle.[24]

3.C. Experimental setup

A clinical ultrasound imaging system (Sonix RP, Ultrasonix Inc., Canada) was used to scan agar phantoms with randomly placed glass beads. The Sonix RP system used a 128 element linear transducer (L14–5/38, Ultrasonix Inc., Canada) with a center frequency measured at 5.5 MHz. The center frequency of the probe was estimated by calculating the spectrum of a signal reflected from a smooth planar Plexiglas surface placed at the focus of the array and facing the array. Figure 1 shows a diagram of the experimental setup used in the experiments. Scans were conducted with the Sonix RP system and radio frequency (RF) data acquired at 40 MHz were stored for postprocessing.

The phantoms were made with 100 ml of degassed water, 2.5 g of agar, and 1.0 g of glass beads (75–90 μm in diameter), and were formed into cylinders with a diameter of 30 mm and height of 15 mm. The phantoms were scanned in distilled, degassed water, and the position of the probe was controlled with a high resolution positioning system (Daedal Inc., Harrison, PA). Depending on the azimuthal focal number used, the phantoms exhibited a scatterer concentration ranging between 2.3 and 3.3 scatterers per resolution cell. Therefore, fully developed speckle was not realized.

3.D. Description of studies

3.D.1. Effects of temperature increase

In simulations, the speed of sound of the background was increased from 1520 to 1540 m/s at 2 m/s increments to replicate effects induced by raising temperature from 37 °C to 48 °C in water.[30] The reflectivities of the individual scatterers were kept constant as a function of temperature in order to isolate the effects of the changes in interference pattern.

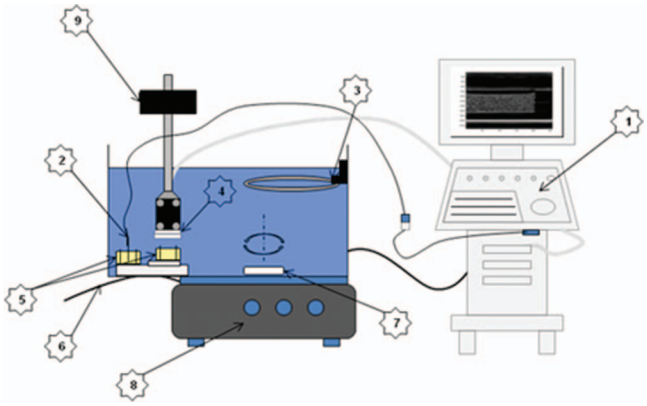

FIG. 1. Configuration of experiment setup: 1. Sonix RP imaging system. 2. Thermocouple. 3. Electric heater. 4. Linear array probe. 5. Phantom used to measure the temperature and phantom being scanned. 6. RS232 serial port cable for communication between the Daedal positioning system and the Sonix RP imager. 7. Magnetic stir bar. 8. Magnetic stirrer. 9. Arm of Daedal positioning system.

In physical experiments, a heating coil (SF30, Waage Electric, Inc, Kenilworth, NJ) was used to adjust the temperature of the water. A magnetic stir bar was used in order to heat the water more uniformly in the tank. A thermocouple was inserted into the phantom outside of the scan region in order to monitor the temperature in the phantom. The Sonix RP was programmed with C++ and LabVIEW to synchronize with the thermocouple to capture frames automatically at every 0.5 °C from 37 °C to 48 °C.

Both simulations and physical experiments were carried out using a receive subaperture of 32 elements. However, transmit subapertures of 32 and 64 elements were used for each trial. The focus was fixed at a depth of 27 mm for all cases and the focus location was not adjusted for changes in the SOS. Rigid and nonrigid registrations were used to compensate for apparent motion.

3.D.2. Elevational displacement study

In both simulations and physical experiments, the probe was displaced in the elevational direction from 0 to 500 μm at a step size of 10 μm. The focal depth was set to 27 mm for all cases. Transmit and receive subapertures both utilized 32 elements. In order to isolate displacement effects for the elevational displacement study, the sound speed in simulations and temperature in physical experiments were kept constant. No registration was used to align each frame because no real or apparent axial motion was observed between frames.

3.D.3. Axial displacement study

In both simulations and physical experiments, the probe was displaced in the axial direction from 0 to 750 μm at a step size of 10 μm. The focal depth was set to 18 mm for all cases. The transmit and receive subapertures both utilized 32 elements. In order to isolate displacement effects in the axial displacement study, the sound speed in simulations and temperature in physical experiments were kept constant. Rigid registration was used to align each frame before calculating the CBE.

4. RESULTS

4.A. Simulations

4.A.1. Temperature simulation

A set of CBE images are shown in Fig. 2 as an example of the positive and negative CBE values that are mapped during increases in temperature. CBE maps or images could also be produced for axial and elevational displacements. The corresponding CBE curves are shown in Fig. 3 using both rigid and nonrigid 2 D cross-correlation tracking. In addition,

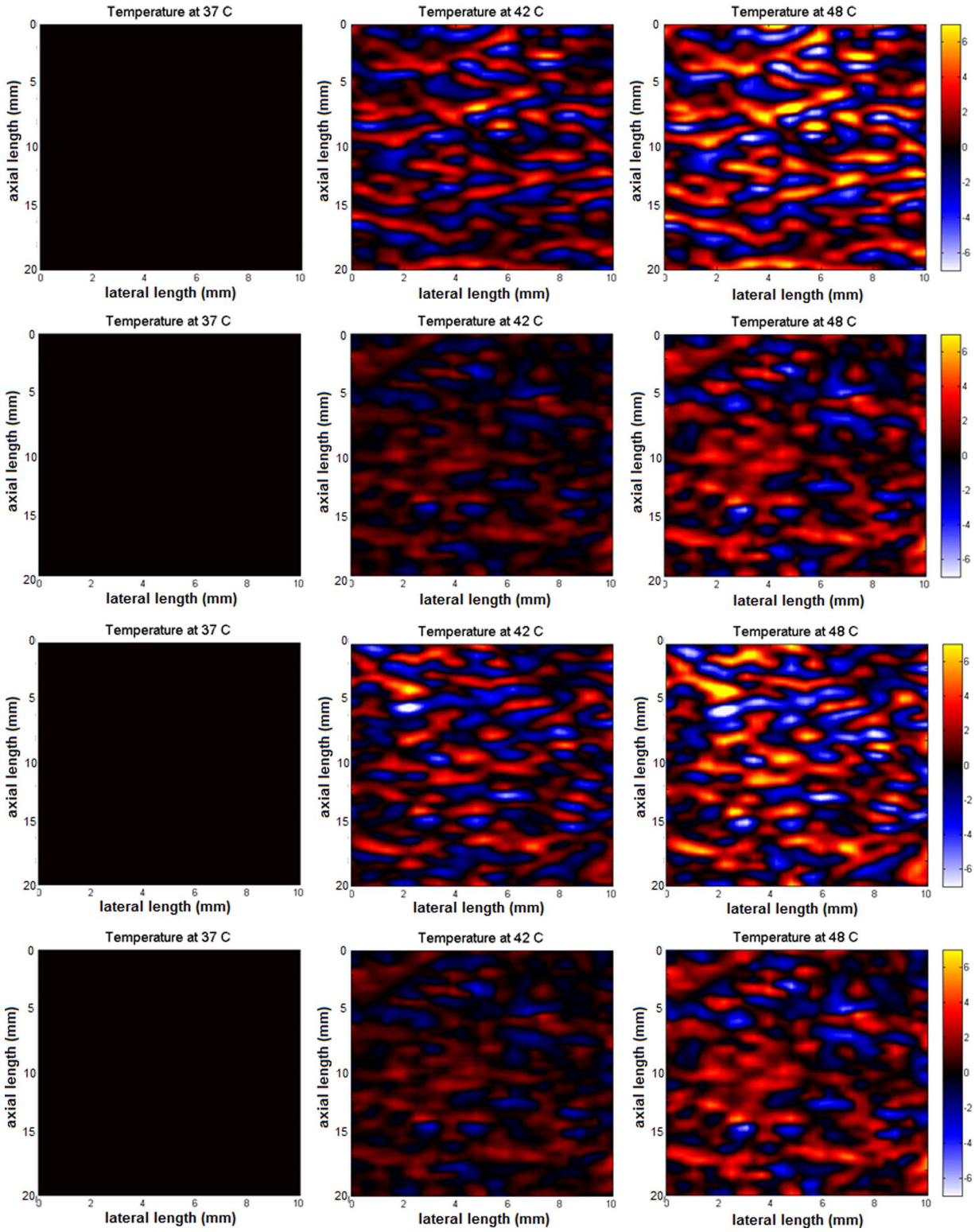

FIG. 2. CBE images of sound speed simulation: First row: Transmitting and receiving with 32 elements with rigid motion tracking method; Second row: Transmitting and receiving with 32 elements with nonrigid motion tracking method; Third row: Transmitting with 64 elements, receiving with 32 elements with rigid motion tracking method; Fourth row: Transmitting with 64 elements, receiving with 32 elements with nonrigid motion tracking method. Scale in dB.

results when using different transmit focal numbers are also provided. Both mean positive and negative CBE curves were generated from the simulations with increasing divergence between the curves as the sound speed increased. Similar behaviors have also been observed in CBE studies involving tissue samples.[19–23] However, the CBE curves in the simulations were not attributable to local changes in scattering properties of lipid and aqueous scatterers. The only changing parameter was the sound speed, i.e., the scattering cross section was set not to change in the simulations.

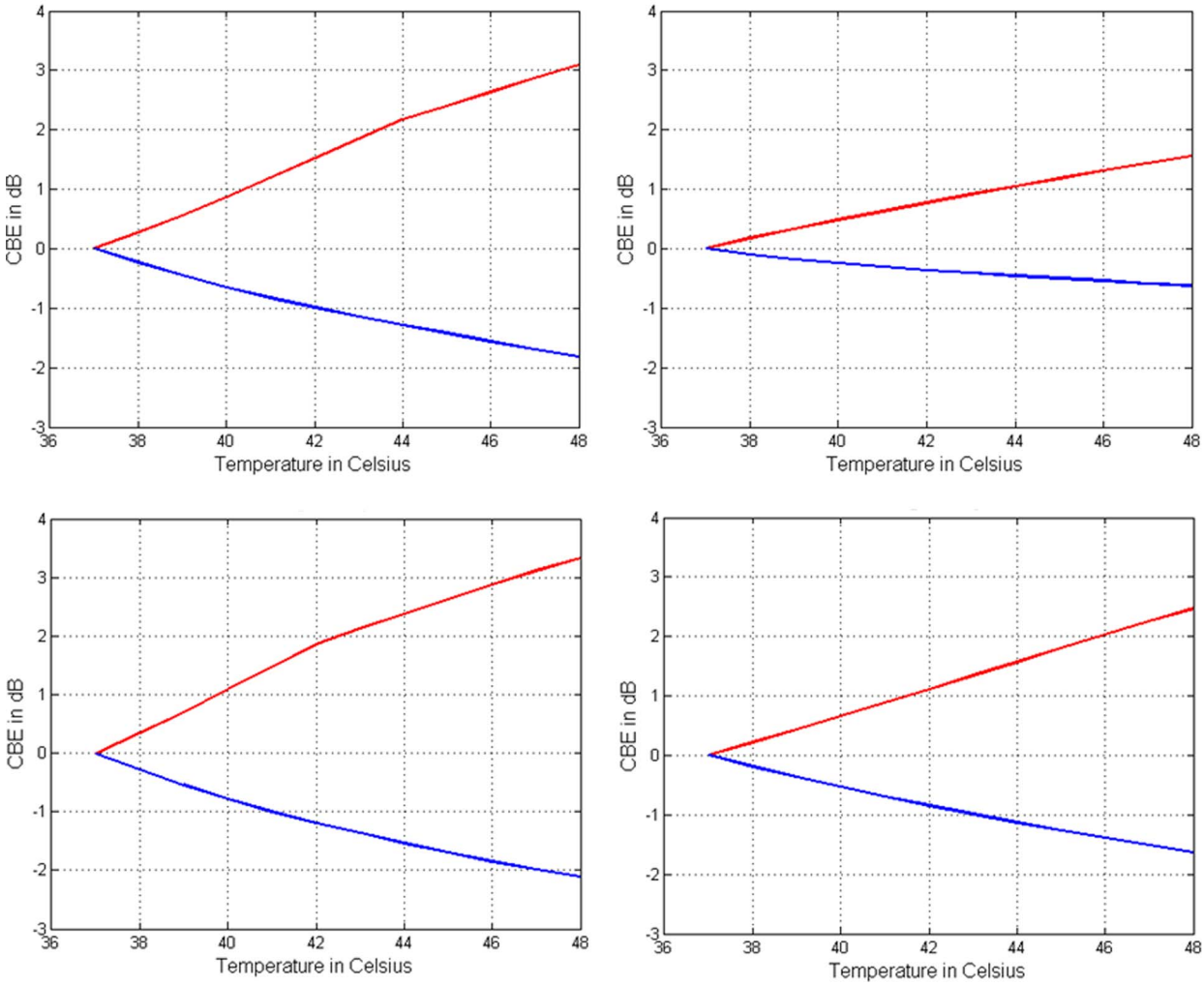

FIG. 3. CBE curves of sound speed simulation: using receive subapertures of 32 (first row) and 64 (second row) elements and both rigid (first column) and nonrigid (second column) registration.

4.A.2. Elevational displacement simulation

Figure 4 shows the CBE curves for the elevational displacements. The divergence between the mean positive and negative CBE curves increased monotonically with the simulated elevational displacement.

4.A.3. Axial displacement simulation

Figure 5 shows the CBE curves for the axial displacement simulations. The divergence between the mean positive and negative CBE curves increased monotonically with the simulated axial displacement.

4.B. Experiments

4.B.1. Temperature experiment

CBE curves from the phantom are shown in Fig. 6. As in the simulations, different motion compensation approaches yielded different results for the CBE curves. To a lesser extent, the use of different focusing parameters on transmit also resulted in different CBE curves. The use of nonrigid registration resulted in smaller changes in the CBE curves. For example, the maximum positive CBE excursion was 2 dB for 32 elements using rigid registration and 1.8 dB using nonrigid

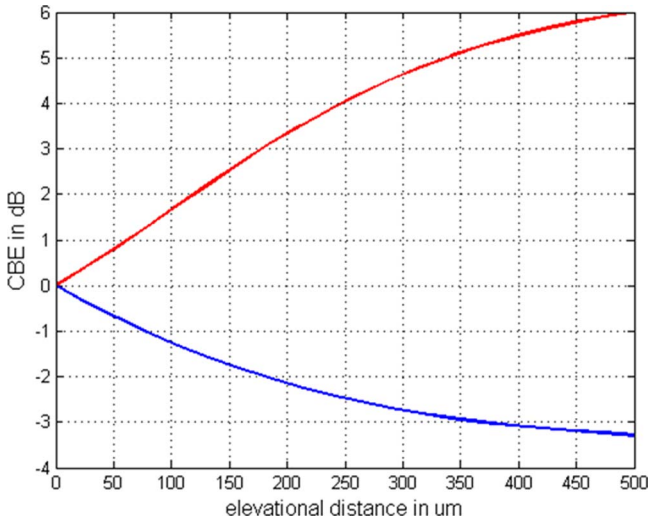

FIG. 4. Elevational displacement simulation CBE curves.

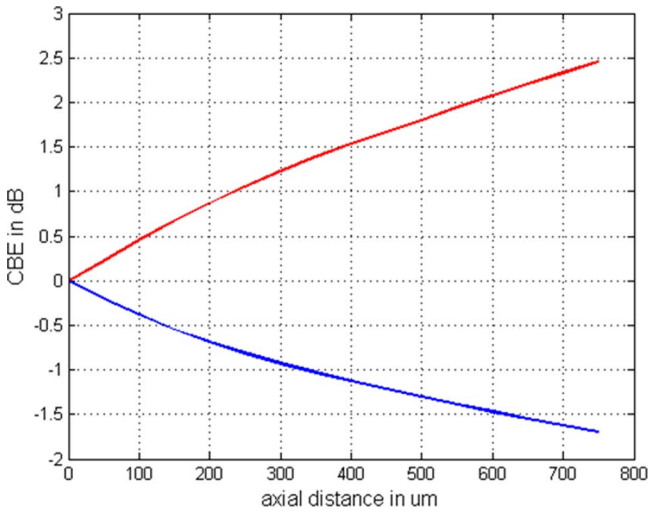

FIG. 5. Axial displacement simulation CBE curves.

registration. When using 64 elements on receive, the maximum CBE excursion was 3.2 dB using rigid registration and 2.2 dB using nonrigid registration.

4.B.2. Elevational displacement experiment

Figure 7 shows the CBE curves corresponding to different elevational displacement values of the probe. As in the simulations, the divergence between the positive and negative CBE curves increased monotonically with the elevational displacement.

4.B.3. Axial displacement experiment

Figure 8 shows the CBE curves constructed by physically moving the probe away from the phantom. As in the simulations, the divergence between the positive and negative CBE curves increased monotonically with the axial displacement.

5. DISCUSSION

5.A. Temperature elevation studies

We hypothesized that an important mechanism producing CBE curves versus temperature was the change in speckle pattern due to changes in the summation of scattered wavelets.

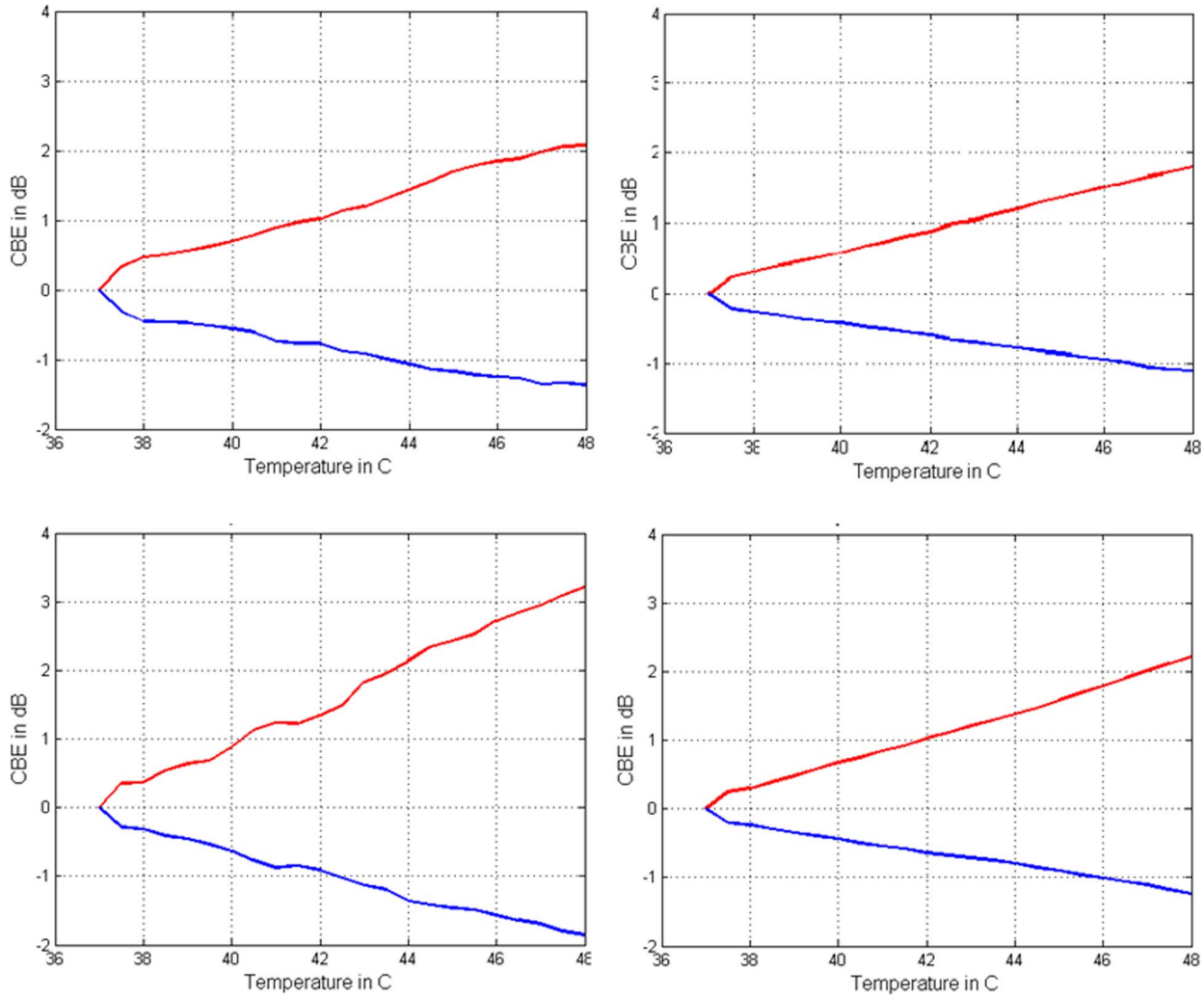

FIG. 6. CBE curves of Temperature experiment: using receive subapertures of 32 (first row) and 64 (second row) elements and both rigid (first column) and nonrigid (second column) registration.

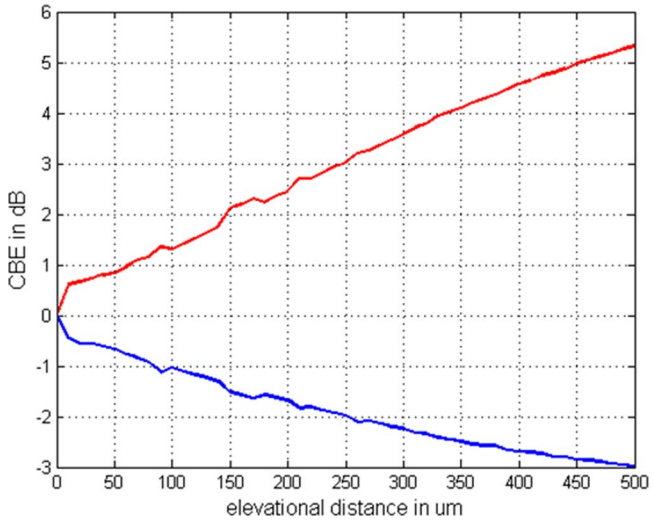

FIG. 7. CBE curves of elevational displacement experiment. The elevational beamwidth at −3 dB is 1.1 mm.

To test this hypothesis, a simulation was conducted in which only the speed of sound was monotonically increased. With only the sound speed changing, CBE curves were generated with similar shape to those produced from studies of temperature elevations in tissue samples.[19–23]

Physical phantoms containing glass bead scatterers were examined versus temperature and their CBE curves were calculated (Fig. 6). Local changes in lipid and aqueous scatterers did not occur during this process. The scattering cross section from the glass beads would not change appreciably over the temperature range of 37 °C–48 °C as both the changes in their acoustic properties (density and sound speed[31]) and radius (volumetric thermal coefficient of expansion $\beta = 27 \times 10^{-6}$ 1/°C, which results in a diameter increase of 0.03% over a 13 °C temperature elevation) should be negligible. Even if the change of scattering cross section of glass beads can contribute to the CBE, the scattering cross section of the glass beads would only either increase or decrease with a monotonic temperature change and would not lead to both positive and negative CBE curves. Further, the experimental CBE curves had excellent agreement (i.e., agreement within 1 dB in the mean CBE values) with the simulation results where only the SOS changed (Fig. 2). Therefore, these changes support the hypothesis that CBE can be due to the changing speckle pattern produced by local changes in summation of scattered wavelets arriving at slightly different times as the SOS changes.

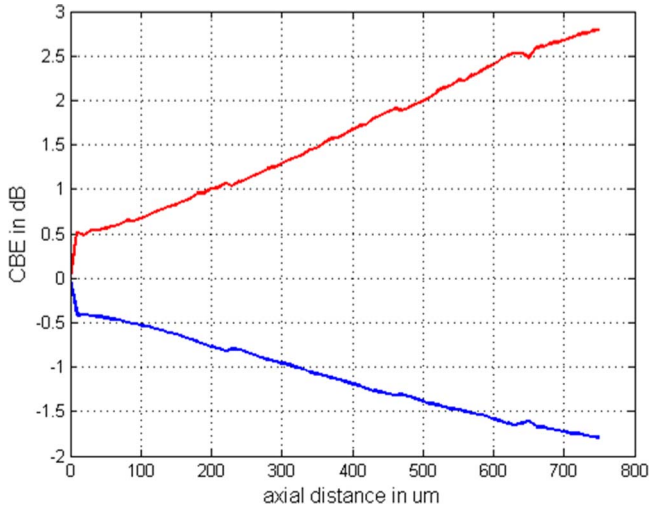

FIG. 8. CBE curve of axial displacement experiment. The focus depth at −3 dB is 9.6 mm.

The effects of different motion tracking methods can be observed in both the simulation and physical experiment results. Increases in sound speed will result in the image shrinking because the arrival times of backscatter wavelets from scatterers in the field will occur more rapidly. The rigid 2D cross-correlation tracking will not compensate for the image shrinkage in axial direction due to the change of speed of sound, thus producing a larger CBE value because the pixels from one frame to the next are not as well aligned as in the case of the nonrigid registration. When nonrigid 2D cross-correlation is applied, the tracking compensates for nonrigid image deformations, thus producing a smaller CBE value. Therefore, these results suggest that the motion tracking method plays an important role in calculating the CBE. However, for a 13 °C temperature increase mean positive and negative CBE values of at least 1.8 and −1 dB, respectively, were obtained regardless of the registration method used.

The effects of different transmitting apertures or transmitting *f* number were also observed in this study, i.e., a smaller *f* number corresponded to a larger CBE change. The spatial gradients associated with the speckle pattern are greater with a smaller *f* number, and therefore changes in the sound speed would result in larger changes in the speckle pattern for more focused transducers. The results of the *f* number study would further support the hypothesis that changes in the speckle pattern due to changes in sound speed are partially responsible for CBE. Therefore, CBE methods for estimating temperature will be dependent on the focal properties of the source. The CBE values should be compensated for changes in focal properties to exclude system dependence.

5.A.1. Elevational and axial motion studies

As Fig. 7 indicates, the change in the speckle pattern produced by elevational displacement of the probe resulted in similar CBE curves to the temperature effect. Even for small elevational displacements, the CBE curves were observed to diverge rapidly. An elevational change of 0.5 mm, which was the maximum displacement recorded, corresponded to about 50% of the beamwidth at the elevational focus. The mean positive and negative CBE values were +5.3 and −3 dB, respectively, when the elevational displacement was 0.5 mm, which was larger than the CBE excursions for the temperature experiments. Therefore, using CBE curves to monitor temperature elevations may not be ideal because any out of plane motion, i.e., elevational shifts, can also produce CBE curves resulting in incorrect estimates of temperature increase.

Perhaps more significant are the results in Fig. 8 showing the CBE curves from the axial motion experiment. The axial shifting of focus caused a change in the local spatial impulse response of the source producing a different speckle pattern that translated into CBE curves. The axial shift corresponded only to approximately 10% of the axial extent of the focal region, but resulted in mean positive and negative CBE values of 2.8 and −1.8 dB, respectively. These results correlated very well with the simulations in Fig. 5, where mean positive and negative CBE values of 2.5 and −1.6 dB, respectively, were obtained. It must be remarked that these CBE values were produced even after registration was performed, which unlike the elevational shift case should produce a perfect motion compensation if the point spread function was to be spatially invariant. Therefore, a sufficiently small axial shifting of the focus can cause CBE curves to be produced and potentially give a false reading for the temperature elevation. The results from both the elevational and axial displacement studies suggest that temperature monitoring using CBE may be very sensitive to motion, and therefore further studies are required to determine the robustness of the technique for clinical applications.

The results presented in this study do not disprove the hypothesis that CBE curves versus temperature can be produced by local changes in aqueous and lipid scatterers. The CBE change was smaller in the temperature experiment using physical phantoms (maximum positive CBE change of 1.6 dB using nonrigid registration at 45 °C) compared to changes observed in experiments in turkey breast[23] over the same temperature regime (maximum positive CBE change of 2.3 dB using nonrigid registration at 45 °C). Therefore, it is possible that the presence of the lipid and aqueous scatterers can magnify the CBE effect (i.e., in the case cited above, this would result in an increase of approximately 18% in the CBE). However, a change in CBE of 18% could result from the different experimental configurations between the study described in this paper and the study detailed in Ref. 23 and, therefore, it cannot be determined if these differences are significant and due to changes in scattering from lipid and aqueous scatterers.

6. CONCLUSIONS

The results presented in this study support the hypothesis that CBE can be produced by changes in speckle pattern resulting from time delays or out of plane motion. This could result from shifts in echo locations due to sound speed changes from temperature elevations or through improperly accounting for motion. However, the current study does indicate that lipid and aqueous scatterers do not need to be present to produce CBE curves. In tissues, such as the liver and turkey breast, the dominant mechanism producing CBE curves, i.e., local changes in lipid and aqueous scatterers or local changes in the temporal location of the summed scattered wavelets, has not been elucidated. Further studies are required to conclude to what degree CBE curves versus temperature are dominated by changes in the temporal location of scattered wavelets and their summation or scattering properties of tissue microstructure.

ACKNOWLEDGMENTS

The authors wish to acknowledge the technical assistance of Jeremy Kemmerer, Adam Luchies, and Billy Ridgway. The work was supported by NIH Grant No. R01 EB008992 (National Institutes of Health, Bethesda, MD) and PUCP Grant No. DGI 2013-0131.

[a]Author to whom correspondence should be addressed. Electronic mail: oelze@uiuc.edu

[1]M. H. Falk and R. D. Issels, "Hyperthermia in oncology," Int. J. Hyperthermia **17**, 1–18 (2001).
[2]E. L. Jones, J. R. Oleson, L. R. Prosnitz, T. V. Samulski, Z. Vujaskovic, D. Yu, L. L. Sanders, and M. W. Dewhirst, "Randomized trial of hyperthermia and radiation for superficial tumors," J. Clin. Oncol. **23**, 3079–3085 (2005).
[3]E. Dikomey and H. H. Kampinga, "Review: Hyperthermic radiosensitization: Mode of action and clinical relevance," Int. J. Radiat. Biol. **77**, 399–408 (2001).
[4]W. Rao, Z. S. Deng, and J. Liu, "A review of hyperthermia combined with radiotherapy/chemotherapy on malignant tumors," Crit. Rev. Biomed. Eng. **38**, 101–116 (2010).
[5]M. D. Hurwitz, "Today's thermal therapy: Not your Father's hyperthermia," Am. J. Clin. Oncol. **33**, 96–100 (2010).
[6]R. Salomir, F. C. Vimeux, J. A. de Zwart, N. Grenier, and C. T. W. Moonen, "Hyperthermia by MR-guided focused ultrasound: Accurate temperature control based on fast MRI and a physical model of local energy deposition and heat conduction," Mag. Res. Med. **43**, 342–347 (2000).
[7]K. Hynynen, "MRI-guided focused ultrasound treatments," Ultrasonics **50**, 221–229 (2010).
[8]B. G. Fallone, P. R. Moran, and E. B. Podgorsak, "Non-invasive thermometry with a clinical x-ray CT scanner," Med. Phys. **9**(5), 715–721 (1982).
[9]A. H. Mahnken and P. Bruners, "CT thermometry: Will it ever become ready for use?" Int. J. Clin. Pract. **65**, 1–2 (2011).
[10]M. Lepetit-Coiffé, B. Quesson, O. Seror, B. D. Senneville, B. L. Bail, C. Moonen, and H. Trillaud, "Real time monitoring of radiofrequency ablation based on MR thermometry and thermal dose in the pig liver in vivo," Eur. Radiol. **18**, 408–416 (2008).
[11]R. Maass-Moreno and C. A. Damianou, "Noninvasive temperature estimation in tissue via ultrasound echo-shifts. Part I. Analytical model," J. Acoust. Soc. Am. **100**, 2514–2521 (1996).
[12]R. Seip and E. Ebbini, "Non-invasive estimation of tissue temperature response to heating fields using diagnostic ultrasound," IEEE Trans. Biomed. Eng. **42**, 828–839 (1995).
[13]C. Simon, P. VanBaren, and E. S. Ebbini, "Two-dimensional temperature estimation using diagnostic ultrasound," IEEE Trans. Ultrason. Ferroelect. Freq. Contr. **45**, 1088–1099 (1998).
[14]T. Varghese, J. A. Zagzebski, Q. Chen, U. Techavipoo, G. Frank, C. Johnson, A. Wright, and F. T. Lee, Jr., "Ultrasound monitoring of temperature change during radiofrequency ablation: Preliminary in-vivo results," Ultrasound Med. Biol. **28**, 321–329 (2002).
[15]M. Pernot, M. Tanter, J. Bercoff, K. R. Waters, and M. Fink, "Temperature estimation using ultrasonic spatial compound imaging," IEEE Trans. Ultrason., Ferroelectr., Freq. Contr. **51**, 606–615 (2004).
[16]M. J. Daniels, T. Varghese, E. L. Madsen, and J. A. Zagzebski, "Non-invasive ultrasound-based temperature imaging for monitoring radiofrequency heating-phantom results," Phys. Med. Biol. **52**, 4827–4843 (2007).
[17]M. D. Abolhassani, A. Norouzy, A. Takavar, and H. Ghanaati, "Noninvasive temperature estimation using sonographic digital images," J. Ultrasound Med. **26**, 215–222 (2007).
[18]A. Anand, D. Savery, and C. Hall, "Three-dimensional spatial and temporal temperature imaging in gel phantom using backscattered ultrasound," IEEE Trans. Ultrason., Ferroelectr., Freq. Contr. **54**, 23–31 (2007).
[19]R. M. Arthur, W. L. Straube, J. W. Trobaugh, and E. G. Moros, "Noninvasive estimation of hyperthermia temperatures with ultrasound," Int. J. Hyperthermia **21**, 589–600 (2005).
[20]R. M. Arthur, J. W. Trobaugh, W. L. Straube, and E. G. Moros, "Temperature dependence of ultrasonic backscattered energy in motion-compensated images," IEEE Trans. Ultrason. Ferroelec. Freq. Contr. **52**, 1644–1652 (2005).

[21]R. M. Arthur, W. L. Straube, J. D. Starman, and E. G. Moros, "Non-invasive temperature estimation based on the energy of backscattered ultrasound," Med. Phys. **30**, 1021–1029 (2003).
[22]R. M. Arthur, W. Straubee, J. Trobaugh, and E. G. Moros, "In vivo change in ultrasonic backscattered energy with temperature in motion-compensated images," Int J. Hyperthermia **24**, 389–398 (2008).
[23]R. M. Arthur, D. Basu, Y. Guo, J. W. Trobaugh, and E. G. Moros, "3-D In vitro estimation of temperature using the change in backscattered ultrasonic energy," IEEE Trans. Ultrason. Ferroelec. Freq. Contr. **57**, 1724–1733 (2010).
[24]R. F. Wagner, S. W. Smith, J. M. Sandrik, and H. Lopez, "Statistics of speckle in ultrasound B-scans," IEEE Trans. Sonics Ultrason. **30**, 156–163 (1983).
[25]C. B. Burckhardt, "Speckle in ultrasound B-mode scans," IEEE Trans. Sonics Ultrason. **25**, 1–6 (1978).
[26]A. Goshtasby, "Image registration by local approximation methods," Image Vision Comput. **6**, 255–261 (1988).
[27]J. M. Fitzpatrick, D. L. G. Hill, and C. R. Maurer, Jr., *Handbook of Medical Imaging* vol 2, (International Society For Optical Engineering Int., Bellingham, WA, 2000), pp. 447–513.
[28]J. A. Jensen, "Field: A program for simulating ultrasound systems," Med. Biol. Eng. Comput. **4**, 351–353 (1996).
[29]J. A. Jensen and N. B. Svendsen, "Calculation of pressure fields from arbitrarily shaped, apodized, and excited ultrasound transducers," IEEE Trans. Ultrason. Ferroelec. Freq. Contr. **39**, 262–267 (1992).
[30]A. D. Pierce, *Acoustics: An Introduction to its Physical Principles and Applications* (Acoustical Society of America, Woodbury, NY, 1994), Chap 1.
[31]J. M. Ide, "The velocity of sound in rocks and glasses as a function of temperature," J. Geol. **45**, 689–716 (1937).